Quantum dynamics of interstitial H_2 in solid C_{60}

S. A. FitzGerald

National Institute of Standards and Technology, Gaithersburg, Maryland 20899
and Department of Physics, Oberlin College, Oberlin, Ohio 44074

T. Yildirim, L. J. Santodonato, D. A. Neumann, J. R. D. Copley, and J. J. Rush

National Institute of Standards and Technology, Gaithersburg, Maryland 20899

F. Trouw

Argonne National Laboratory, Intense Pulsed Neutron Source, Argonne, Illinois 60439
(Received 27 January 1999)

We present a neutron-scattering study of the quantum dynamics of molecular hydrogen trapped inside solid C_{60}. The loading isotherm is shown to deviate significantly from a standard Langmuir response and follows instead an exponential form, increasing from 40% filling at 130 atm to 90% at 700 atm. Diffraction data confirm that the adsorbed molecules are randomly oriented and sit exclusively at the octahedral site. Inelastic neutron scattering clearly shows the ortho to para conversion of the interstitial hydrogen, which occurs via a transition from the $J=1$ to $J=0$ rotational levels. The level scheme shows relatively minor deviations (on the order of a few percent) from the free rotor model with the splitting in the excited level being the same, 0.7 meV, for both H_2 and D_2. In contrast the shift in the overall level, which is shown to depend critically upon zero-point motion is almost three times greater for H_2 than D_2. We also identify the translational modes of the trapped molecules which occur at a much higher energy than would be classically predicted and have an isotopic shift on the order of $\sqrt{2.2}$. Quantum-mechanical model calculations within the *self-consistent harmonic* approximation indicate that zero-point motion of H_2 molecules in the ground state play the central role in understanding the experimental results, and in particular the high energy of the translational modes and the magnitude of their isotopic shift. [S0163-1829(99)03133-1]

I. INTRODUCTION

Due to their large spherical shape, C_{60} molecules form an fcc lattice in which there are two tetrahedral (T) and one octahedral (O) interstitial site per molecule. These sites are large enough to accommodate a variety of atomic and molecular species, the presence of which can significantly influence the properties of C_{60}. Most notable are the alkali-doped C_{60} compounds which display superconductivity at reasonably high temperature. More recent studies have looked at the behavior of less reactive dopants showing that He, Ne, H_2, N_2, H_2O, CO, and O_2 all enter into the C_{60} lattice interstitially,[1–6] however relatively little has been done on understanding the nature of the interactions with the trapped species.

In this paper we report a neutron-scattering study of the low-temperature dynamics of molecular hydrogen trapped in the interstitial sites of C_{60}. The molecules form an almost perfect example of a three-dimensional quantum rotor in a solid with energy levels given by

$$E_J = BJ(J+1), \qquad (1)$$

where B is the rotational constant and J is the rotational quantum number. Due to the simplicity of the model it is easy to probe the effects of relatively weak interactions with the host lattice which lead to a departure from free rotor behavior. This in turn leads to accurate information about the symmetry of the host and the nature of the intermolecular

interactions between the hydrogen and the C_{60} molecules. The inherent quantum nature of the resultant dynamics makes this study of particular interest and the large incoherent scattering cross section of hydrogen, makes inelastic neutron scattering (INS) the ideal tool to study the behavior.

Since H_2 is composed of two indistinguishable fermions the rules of quantum statistics constrain it to have an overall antisymmetric wave function. If the spin part of the wave function is antisymmetric under exchange of nuclei then the spatial part must be symmetric. And similarly if the spin part is symmetric then the spatial part must be antisymmetric. This leads to two kinds of hydrogen: para H_2, which is the minority species at room temperature, has even values of J and antiparallel nuclear spins, and ortho H_2, the majority species with odd values of J and parallel nuclear spins.[7] These properties are summarized in Table I.[7] At low temperature in the condensed phases only the $J=0$ and $J=1$ levels are thermally populated. Because relaxation to the energetically favorable para state can only occur via a flipping of the nuclear spin, ortho H_2 persists for long periods of time (on the order of days for pure H_2) even at the lowest of temperatures. In the absence of any relaxation the ratio of ortho to para molecules remains fixed at the room-temperature value which is simply determined by the statistical weight of the the two species. At low temperature 3/4 of the molecules are trapped in the $J=1$ ortho state.

In a similar way, D_2 which is composed of two indistinguishable bosons is also subject to constraints such that the overall wave function must be symmetric under exchange of

TABLE I. Symmetery properties of the hydrogen isotopes. I refers to the nuclear spin and J to the molecular rotational quantum number.

Isotope	I_{Mol} (Symmetry)	J (Symmetry)	Nuclear weight	Species
Hydrogen	0 (AS)	0,2,4,6, . . . (S)	1	Para
(fermion $I_N = 1/2$)	1 (S)	1,3,5,7 . . . (AS)	3	Ortho
Deuterium	0 (S)	0,2,4,6 . . . (S)	1	Ortho
(boson $I_N = 1$)	1 (AS)	1,3,5,7 . . . (AS)	3	Para
	2 (S)	0,2,4,6 . . . (S)	5	Ortho

the two nuclei. For D_2 the symmetric spin states occur for I, the total molecular nuclear spin equal to either 0 or 2. As shown in Table I this leads to 2/3 of the molecules having even values of J and 1/3 having odd. In the absence of any relaxation 1/3 of the molecules will be trapped in the $J=1$ state at low temperature. Since this is the minority species (as opposed to H_2 where $J=1$ is more abundant) it is referred to as the para state. Finally, we note that for both H_2 and D_2 all other excitations of comparable energy which do not involve a conversion between ortho and para states are rapidly ''frozen out'' at low temperature. Hence incoherent neutron scattering, which can flip the nuclear spin via the magnetic moment of the neutron, is able to probe the rotational ortho and para conversions without contamination from any other excitations.

In the orientationally disordered phase of C_{60} the potential felt by H_2 molecules in the O site has O_h symmetry, leading to an accidental degeneracy among the $J=1$ levels. However, in the low-temperature $Pa\bar{3}$ structure, the symmetry of the potential is lowered to S_6 and the degeneracy is removed. Thus the magnitude of the splitting in the $J=1$ level depends directly upon the order parameter of the C_{60} lattice.

In the next section we describe the sample preparation and data taking techniques. The experimental results are presented in Sec. III. We first present the elastic neutron-scattering results in which a ''difference Fourier transform'' analysis of the $C_{60}(D_2)_x$ diffraction data clearly shows the D_2 molecules situated randomly at the O sites without any long-range order. The inelastic neutron-scattering results are shown for both D_2 and H_2 doped samples. The D_2 data is shown first since the various excitations are well separated in energy making the analysis more straightforward. The results indicate that the interstitial hydrogen forms a somewhat unique system in which the potential is quite rigid for center-of-mass translation while at the same time being very soft for rotational motion. The hydrogen molecules are shown to rotate quite freely with relatively small perturbations being introduced by the interactions with the host lattice. However, the lack of any significant recoil effect even at temperatures as high as 200 K allows us to the conclude that the molecules are translationally confined within the interstitial site. This is further confirmed by the existence of very high-energy translational modes in which the entire hydrogen molecule vibrates relative to the C_{60} lattice. Despite the large size of the O site, these translational modes of are found to be comparable in energy to that of the rotational transition from $J = 1$ to $J = 0$.

In the analysis section we show that this unusual behavior is due to the large zero-point motion of the H_2 molecules in the O site, leading to a significant departure from the classically predicted interactions. In our model calculations, the hydrogen-carbon interactions are expressed as a simple 12-6 potential within a *self-consistent harmonic* approach to show that the splitting in the rotational mode results from the interaction with the host lattice while the shift in energy is predominantly due to the coupling between the rotational and zero-point motion of the hydrogen. Examination of data for both D_2 and H_2 confirms the models predictions for translational modes, the magnitude of their isotopic shift, and the lack of any recoil effect in the rotational transitions.

II. EXPERIMENTAL TECHNIQUE

The sample consisting of 10 g of commercially obtained pure C_{60} powder was first heated under vacuum at 450 K for 2 days to remove any traces of solvent. The powder was sealed inside a high-pressure aluminum cell, the system was evacuated and hydrogen gas was introduced directly from a standard cylinder at a pressure of 130 atm. In those cases where a higher loading pressure was desired the gas was introduced at temperatures as low as 50 K. The system could then be isolated and heated back to room temperature to achieve pressures on the order of 750 atm. Our results indicate that maintaining the pressure for 5 h with the sample kept at a temperature of 323 K was sufficient to achieve complete loading for the given pressure. Once loaded, the sample was cooled below 150 K thereby ''freezing'' the interstitial H_2 inside the C_{60} lattice. At that point all the free gas around the sample could be pumped away. After completion of the neutron-scattering experiments the sample was again heated to 330 K. Over the course of 24 h the trapped hydrogen was allowed to outgas into a vessel of known volume and hence the quantity of hydrogen that was originally trapped in the lattice was determined. The diffraction data were obtained using the NIST 32-detector high-resolution powder diffractometer at BT-1.[8] Scans were taken over a period of 24 h with the sample at a temperature of 10 K and the diffractometer operating at a wavelength at 1.54 Å. The incoherent inelastic neutron-scattering data were obtained using the NIST Fermi-Chopper time-of-flight (TOF) spectrometer.[9] An incident beam monochromated by double Bragg reflection from two pyrolytic graphite (002) crystals to a wavelength of 4.8 Å was used to produce a resolution of 0.14 meV at the elastic position. At high-energy gain the resolution of the spectrometer increases roughly linearly with energy leading to a resolution of 1.1 meV for an energy gain of 15 meV.

III. EXPERIMENTAL RESULTS

A. Loading isotherms

The loading isotherm data were obtained at 323 K with the C_{60} powder exposed to a constant pressure of H_2 gas for 5 h. The quantity of H_2 loaded into the sample was determined by measuring the outgassing from the sample after first removing all external gas at low temperature. The accuracy of this technique was confirmed by neutron-diffraction analysis. The two methods showed the same site occupancy
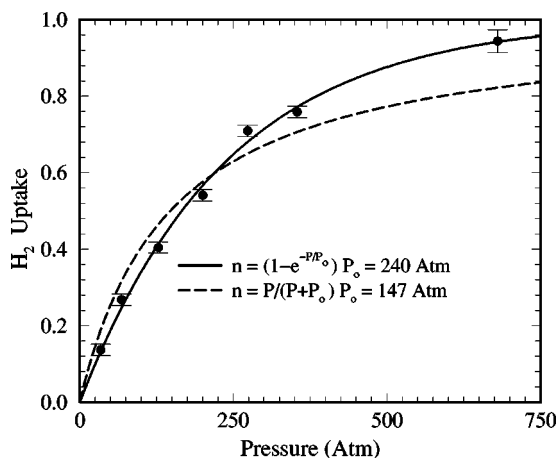
FIG. 1. Isothermal loading pressure curve (dots) at 323 K for H$_2$ in C$_{60}$. The solid line is obtained from the empirical relation $n = 1 - \exp(-P/P_0)$ with $P_0 = 240$ atm. The dashed line shows the best fit to the data based on Langmuir isotherm $n = P/(P + P_0)$.

FIG. 2. Neutron powder-diffraction pattern (dots) of C$_{60}$(D$_2$)$_x$ taken at 10 K, a Rietveld profile refinement (solid curve) (Ref. 13) based on pure C$_{60}$ model with D$_2$ occupying the octahedral sites, and a difference plot (bottom). The inset shows how the goodness of the fit (weighted R factor) changes with the occupancy of the octahedral D$_2$. The best fit with a weighted R factor of 8.9% is obtained when 40% of the octahedral sites are filled.

to within 2% absolute, for a standard loading pressure of 130 atm. Figure 1 shows the results expressed in terms of the fraction of O sites that are filled for a series of loading pressures ranging up to 750 atm. In agreement with Henry's Law, at low pressures the loading isotherm approaches linearity with a Henry constant of 0.4 atm^{-1}. The occupancy increases smoothly with pressure before saturating at a value approaching 100%. As shown in Fig. 1 the data follow very closely to the simple empirical equation

$$n = 1 - \exp(-P/P_0) \qquad (2)$$

with $P_0 = 240$ atm. In comparison Ne, which follows the same functional form, has a value of $P_0 = 990$ atm[4]. The physical origin of this functional form is not clear to us at the moment. Most sorption systems are very well described by the standard *Langmuir isotherm*

$$n = P/(P + P_0), \qquad (3)$$

which is linear in the pressure at low concentration, with a probability constant $(1/P_0)$ that depends exponentially on the binding energy to the sorption site. The Langmuir isotherm is based on a noninteracting lattice-gas model with the assumptions that (1) each adsorbed molecule has a sorption potential energy ϵ_0, which is independent of both loading pressure and the amount of loading; (2) the host lattice (i.e., C$_{60}$) has N sites (i.e., O sites), each of which may have either 0 or 1 molecules; and (3) the adsorbed atoms are distributed randomly over the sites and do not interact with each other. It might appear that these assumptions are valid for the C$_{60}$-H$_2$ system however, the results shown in Fig. 1 indicate that the Langmuir isotherm produces quite a poor fit to the experimental data (dashed line). A possible reason for the failure of the Langmuir isotherm could be that the binding energy ϵ_0 has a small pressure dependence. Similarly the interactions between the adsorbed H$_2$ molecules, although small are not negligible, and this could also lead to a departure from a Langmuir behavior. Currently, we are considering how to incorporate these ideas into a more complete theoretical model.
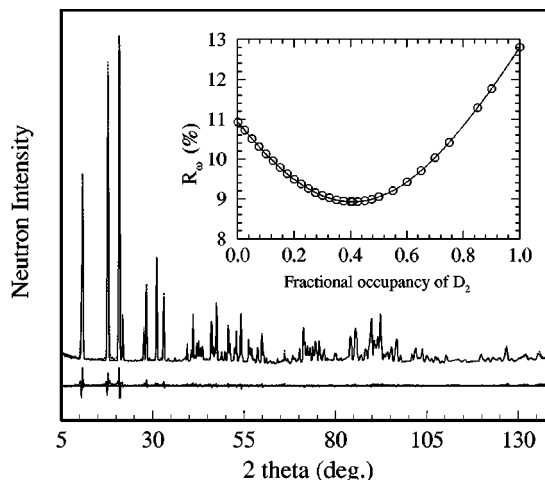
B. Diffraction data

The fcc structure of solid C$_{60}$ has two T and one O interstitial site per molecule. The T site has an effective radius of 1.13 Å while the O site is 2.06 Å.[1] Since hydrogen has a van der Waals radius of 1.2 Å,[10] we would not expect it to occupy T sites, at least at the moderate pressures used in this study. In our case the location of the interstitial molecules is determined by neutron powder diffraction. Due to the large incoherent cross section of H$_2$ the diffraction data were obtained on a sample of C$_{60}$ doped with D$_2$. The resulting powder pattern taken at 10 K along with the final Rietveld refinement is shown in Fig. 2.

The initial refinement of the diffraction data, was performed using the the model of David *et al.*[11,12] for pure solid C$_{60}$ without any consideration of the D$_2$ molecules.[13] The refined values of the carbon positions, molecular orientations, temperature factors, etc. were all found to be very similar to those of pure C$_{60}$, indicating that the presence of D$_2$ does not affect the lattice structure significantly. The overall agreement with the data was reasonably good leading to a weighted R factor (goodness of fit) of 11%.[13] However, it was clear that a significant scattering density was absent from the refinement. In order to determine the location of this missing scattering density, we calculated the *difference Fourier transform* between the data and the pure C$_{60}$ refinement model. A continuous contour plot of this *difference Fourier transform* in the (100) plane is shown in Fig. 3. The intense spots located at the O sites show quite dramatically that the missing scattering density is located at the O sites.

A complete analysis of the data in which we refined the occupancy of D$_2$ in both the O and T sites confirmed a zero-site occupancy for the T site and a finite occupancy for the O site.[14] The goodness of fit (R factor) as a function of O occupancy is shown in the inset to Fig. 2. For the test sample the best fit with a weighted R factor of 8.9% was obtained for a D$_2$ occupancy of roughly 40%. The improvement in the weighted R factor is quite significant and the 40% occupancy
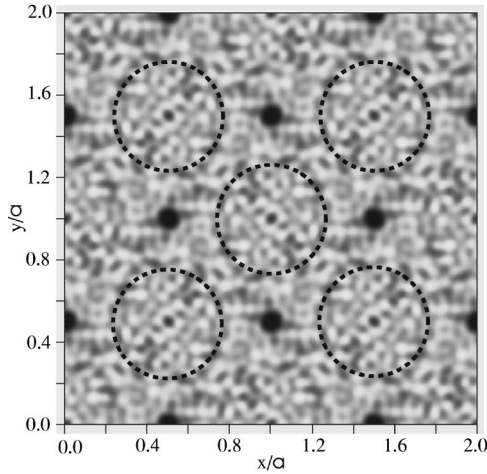
FIG. 3. A difference Fourier transform between the Rietveld refinement model of pure C_{60} (without D_2) and the neutron powder-diffraction pattern of $C_{60}(D_2)_x$ shown in Fig. 2. Continuous contour plot shows the residual scattering density in the (100) plane. The excess scattering density (dark spots) illustrate very clearly that the D_2 molecules are randomly oriented in the octahedral sites. The dashed circles have been added to show the location of the C_{60} molecules.

number is in good agreement with the outgassing results discussed in the previous section.

The powder-diffraction pattern, did not show any super-lattice peaks associated with ordering of D_2 in O sites and hence we conclude that (1) the D_2 molecules occupy the O sites in a random fashion without any long-range ordering and (2) the presence of D_2 in solid C_{60} causes only minor perturbation to the structure of the host lattice as would be expected from the large size of the O sites. The refinement also indicated that the root-mean-square (rms) thermal displacement of D_2 in O sites was on the order of $\langle u^2 \rangle \approx 0.15$ Å^2, which is unusually large for a temperature of 10 K. We believe that this large value of $\langle u^2 \rangle$ is mainly due to zero-point motion of the D_2 molecules in the large cavities of the O sites. In the next section we show that this behavior is confirmed by the inelastic-scattering results.

C. Inelastic neutron-scattering results

1. D_2 in C_{60}

The inelastic neutron scattering was performed on C_{60} powder in the same cell and prepared under the same condition as those used for the diffraction study. D_2 having twice the mass of H_2 but the same internuclear separation has a rotational constant which is half that of H_2 and therefore its $J=1$ to $J=0$ transition occurs at 7.35 meV.[15] Deuterium's relatively low incoherent neutron cross section required us to average the data for three days, while keeping the sample at 10 K for the whole time. Figure 4 shows the TOF neutron energy gain spectrum of C_{60} with a 40% D_2 occupancy in the O site. The results have been integrated over all detectors covering a Q range from 2 to 4 Å^{-1}. The rotational transition is seen to have been split into two peaks centered at 7.4 and 6.7 meV with a full width at half maximum (FWHM) of 0.6 and 0.5 meV, respectively. Since the resolution of the spectrometer is energy dependent both peaks are in fact reso-
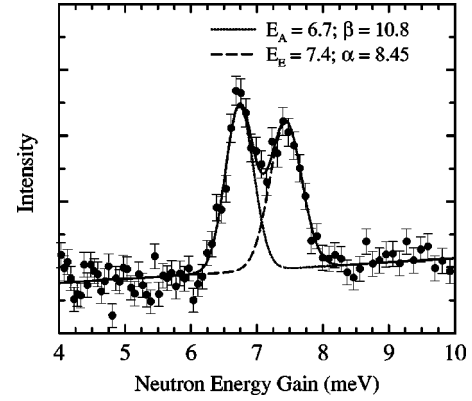

FIG. 4. Time-of-flight neutron energy gain data taken on a $C_{60}(D_2)_x$ sample at 10 K. The data is fit to two Gaussian peaks centered at 7.4 and 6.7 meV using Eq. (4).

lution limited. As we explain in the analysis section, the interactions with the C_{60} lattice cause the $J=1$ rotational level to be split into an E state with a degeneracy of two and an A state with a degeneracy of one. The intrinsic ratio of the transition strength to the ground state is thus $2:1$. However, the ratio of the observed intensity is modified by the thermal population factor such that the spectrum is modeled as

$$I = I_{BG} + I_0 (2 e^{-(E_E - E_A)/k_B T} e^{-\alpha(E - E_E)^2} + e^{-\beta(E - E_A)^2}),$$

(4)

where I_{BG} is the background correction, I_0 is the overall scaling factor for the two peaks, E_E and E_A are the energy of the doublet and singlet mode, respectively, and α and β determine their FWHM. The fit shown in Fig. 4 is quite good, and indicates a splitting of 0.7 meV with the overall center of mass of the para to ortho transition situated at 7.2 meV, a shift of 0.15 meV relative to free D_2.

Figure 5 shows the TOF data at higher temperatures referenced to that of the pure C_{60} sample. The two peaks at 7 meV are still present, however, with increasing temperature the spectra are dominated by a broad feature centered at 9.2 meV. The fact that the strength of the 7 meV peaks show almost no temperature dependence further confirms that they arise from a para to ortho rotational transition. A 7 meV
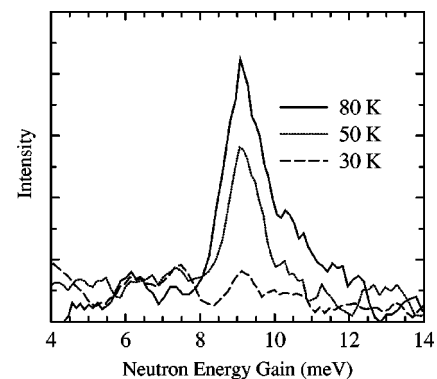

FIG. 5. Time-of-flight neutron energy gain data taken on a $C_{60}(D_2)_x$ at a series of temperatures. Each curve has been referenced to that of a pure C_{60} sample. Error bars have been omitted for clarity but are on the order of the noise that is present in the base line.
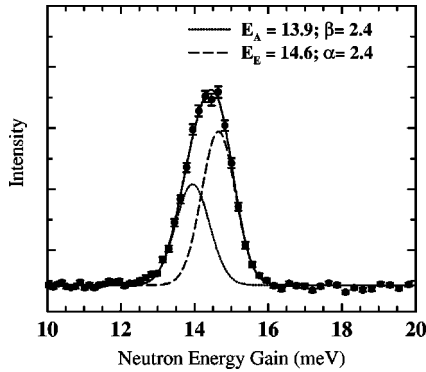
FIG. 6. Time-of-flight neutron energy gain data taken on a $C_{60}(H_2)_x$ sample at 30 K. The data is fit to two Gaussian peaks centered at 13.9 and 14.6 meV using Eq. (4).

excitation in a system which is in thermal equilibrium would increase in strength by more than three orders of magnitude on changing temperature from 10 to 80 K.

In contrast to the behavior of the rotational transitions we see that the 9.2 meV peak, which is negligible at 10 K does increases in strength between 30 and 80 K in accordance with the well-known thermal Bose factor. This thermal behavior and the energy of the peak are both consistent with a translational mode in which the D_2 molecule as a whole vibrates against the C_{60} lattice. This will be discussed in more detail in the analysis section. Finally, we note that the 9.2 meV peak has a definite asymmetry suggesting that it is composed of at least two modes in the region of 9–10 meV.

2. H_2 in C_{60}

Figure 6 shows the neutron energy gain spectrum of C_{60} loaded with 40% H_2. Although the spectrum consists of just the one peak centered at 14.3 meV, an examination of Eq. (4) shows that the data can be modeled by two resolution-limited peaks at 13.9 and 14.6 meV, respectively. The splitting of 0.7 meV is in fact the same as that of D_2 and it is merely the fact that the spectrometer has a much lower resolution (1.1 meV at 15 meV) at higher energy that makes the transition appear as a single peak. The center of mass at 14.35 meV is almost double our results for D_2 and corresponds to a shift of 2.4% from that of pure hydrogen at 14.7 meV.[16] The relatively small shift in energy implies that the interstitial hydrogen is rotationally quite free. However, the fact that the peaks are still resolution limited at a temperature of 30 K indicates that the hydrogen is translationally bound to the lattice. If the hydrogen were not bound, the recoil effect from the neutron impact would lead to a broadening of up to 16 meV for the Q range covered in our experiment.

Figure 7 shows the temperature dependence of the energy gain spectrum. The main peak appears to shift slightly to lower energy with increasing temperature while broadening from a FWHM of 1.4 meV at 30 K to 4.2 meV at 200 K. However, this could also be explained in terms of the shoulders on both the high- and low-energy sides of the main peak which become stronger with increasing temperature. In addition to the main peak, all the higher temperature spectra contain a secondary peak centered at 28.0 meV. This is in the correct energy range for the $J=2$ to $J=1$ rotational transition which occurs at 29.4 meV in free hydrogen. However,
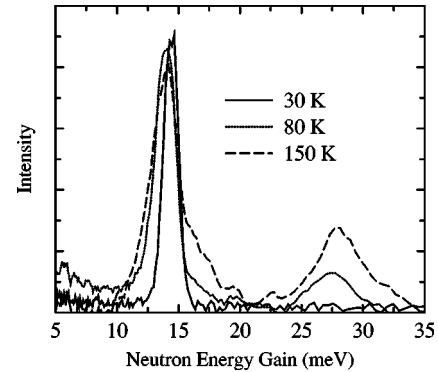

FIG. 7. Time-of-flight neutron gain data taken on a $C_{60}(H_2)_x$ at a series of temperatures. Each curve has been referenced to that of a pure C_{60} sample. Error bars have been omitted for clarity but are on the order of the noise that is present in the base line.

for this transition to occur, the $J=2$ level at 44 meV has to be thermally populated. At 80 K, less than 0.1% of the para molecules would be excited into the $J=2$ level and hence the transition strength should be negligible. Another puzzle connected with Fig. 7 is the absence of any obvious features corresponding to the 9–10 meV translational peaks in the D_2 spectrum. For a translational mode the simple isotopic shift of $\sqrt{2}$ predicts that there should be peaks in the H_2 spectrum in the region of 13–14 meV. It is possible that interactions with the lattice could have modified the isotopic shift such that the translational modes occur close enough in energy to the rotational peaks for the two excitations to appear as one broad feature in the high-temperature spectra shown in Fig. 7. In contrast to the behavior for D_2 we would not expect the H_2 translational modes to dominate at higher temperatures since the ratio of the incoherent to coherent scattering cross section is extremely large in H_2 thus enhancing the strength of its rotational transitions relative to the translational modes.

In an attempt to isolate the translational modes of the H_2 doped sample, we used energy-loss measurements which can observe these modes even at the lowest temperature. The measurements were performed on the QENS spectrometer at Argonne National Laboratory which has a better energy resolution of 0.3 meV at 14 meV. The results presented in Fig. 8, show at least three features centered at 13.4, 14.2, and 14.9 meV, respectively. It appears that these features result from various translational modes plus the two rotational transitions observed in the neutron energy-gain spectra. However,
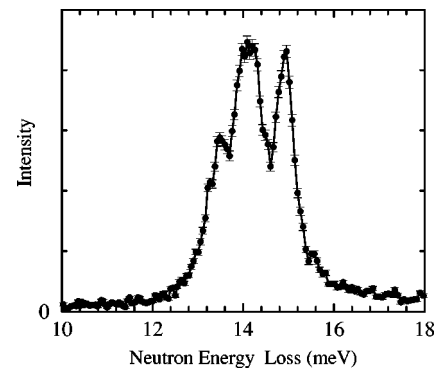

FIG. 8. QENS neutron energy loss data taken at 4.2 K. The curve is the sum of scattering at angles of 40, 90, and 130 degrees.
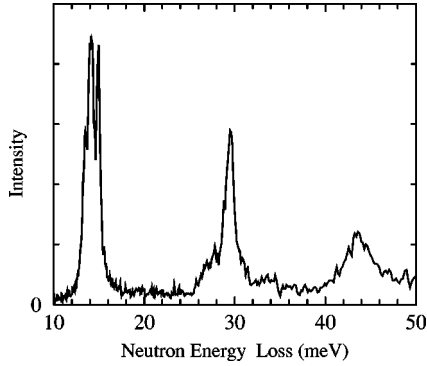
FIG. 9. QENS neutron energy loss data at 4.2 K shown over an extended energy range. Error bars have been omitted for clarity but are on the order of the noise that is present in the base line.

FIG. 10. A schematic representation of the local environment of a H_2 molecule trapped in the octahedral site of solid C_{60}. The large black spheres represent C_{60} molecules. The large grey sphere indicates the void in the octahedral site in which H_2 molecule performs zero-point vibration. As discussed in the text, all calculated physical quantities are renormalized significantly due to this zero-point vibration.

none of the peaks are completely resolved and it is still not possible to assign specific features to specific modes. It would have been useful to perform similar measurements on a $C_{60}(D_2)_{0.4}$ however a predicted beam time requirement on the order of 10 days made this impractical. The extended picture of the QENS loss data shown in Fig. 9, contains broad features at 29 and 44 meV. The peak at 29 meV shows definite evidence for more than one component and it is quite likely that one of these is the result of a transition from the $J=1$ to $J=2$ rotational states. It would however, be impossible for the 44 meV peak to arise from either a $J=2$ to a $J=3$ rotational transition ($J=2$ level is not populated at 4.2 K) or from a $J=0$ to a $J=2$ rotational transition which can only occur via coherent scattering and would be too weak to account for the intensity of the observed peak.[17] It now appears that these higher energy features are the result of multiphonon transitions involving the translational modes. This is consistent with the data in that each higher-order process is broader and less intense than the previous.

IV. ANALYSIS AND DISCUSSION

A. The potential function

In this section, we present quantum-mechanical calculations of the dynamics of H_2 molecules trapped in the O sites of solid C_{60}. We assume that the C_{60} molecules are located on a fcc lattice in their equilibrium $Pa\bar{3}$ orientations and that the dynamics of the interstitial H_2 are determined by the external potential produced by the surrounding C_{60} molecules. The local environment of a H_2 molecule in the octahedral site is schematically shown in Fig. 10. We ignore the interactions between H_2 molecules as well as the effect of H_2 on the host lattice. Hence, our model neglects cooperative effects which should have essentially no influence on the rotational and vibrational excitations of individual H_2 molecules. We also neglect the minor orientational defects observed in C_{60} in the following analysis. In the present work, our first goal is to determine those properties that can be explained without introducing any second-order effects due to the minor orientational disorder. We note that the difference in the relative orientation of the C_{60} molecules between the major and minor $Pa\bar{3}$ orientations is very small (pentagonal faces become hexagonal and vice versa) and hence,
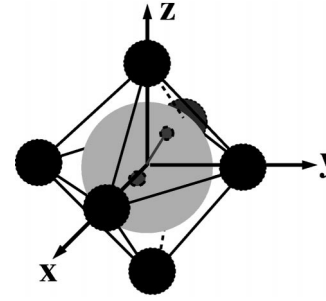
the local crystal field is expected to be largely unaffected by the presence of molecules with minor orientations.

The potential felt by a H_2 molecule in the octahedral site can be modeled in terms of a van der Waals interaction with the six surrounding C_{60} molecules. This is well described by an atom-atom potential given by

$$V(\mathbf{R},\mathbf{\Omega}) = \sum_{i \in H_2} \sum_{j \in C_{60}} \{Be^{-Cr_{ij}} - A/r_{ij}^6\}, \quad (5)$$

where $\mathbf{R}$ and $\mathbf{\Omega} = (\theta, \phi)$ are the position vector of the center and the orientation of the molecule, respectively, and A, B, and C are the appropriate parameters for the C-H interaction. A (the van der Waals contribution to the interaction between C and H) can be estimated from the London formula;[18] $A = -\frac{3}{2}\alpha_C\alpha_H[I_CI_H/I_C+I_H] \approx 5.53$ eV Å^6, where α and I are the atomic dipole polarizabilities and ionization potentials, respectively.[18] B and C in the repulsive term of the potential (the exchange contribution) are usually estimated by fitting a large number of experimental data on similar systems. Pertsin and Kitaigordsky[18] list various values for the parameters A, B, and C derived using different models. In this work we use, without any modification the parameters obtained via the WS77 model in which $A = 5.941$ eV Å^6, $B = 678.2$ eV, and $C = 3.67$ Å^{-1}. We also confirmed that the results reported here do not change significantly if other potentials given in Ref. 18 are used.[19] Starting from this simple potential model we use a self-consistent harmonic (SCH) approach to develop a perturbative theory for the crystal-field splitting of the rotational J levels of a rigid H_2 molecule. We also show that the interactions give rise to a significant coupling between the rotational motion of the H_2 molecules and the center-of-mass (CM) vibrations, which proves to be essential in explaining the experimental data.

B. Center-of-mass motion

First, we examine the variation in the potential with respect to the CM position of a H_2 (or D_2) molecule. Due to the large octahedral site, the weak van der Waals interactions, and the light mass of H_2 we would expect the molecule to have a large zero-point motion. The system, therefore, needs to be treated using quantum-mechanical techniques in
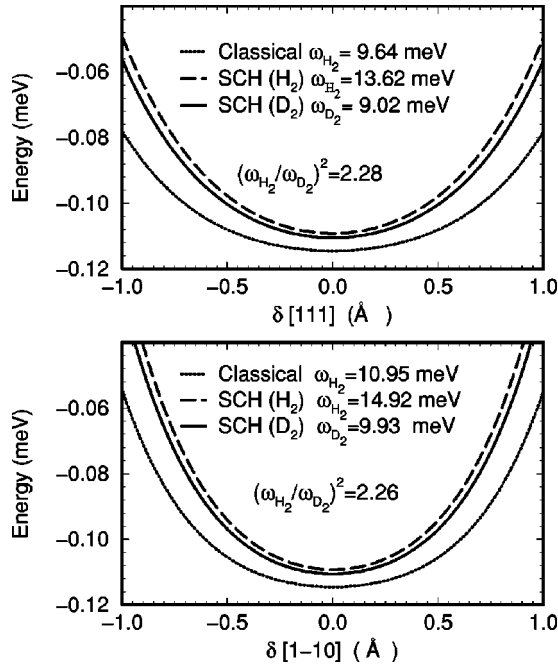
FIG. 11. Potential energy as a function of the position of the center of a para-H$_2$ molecule ($J=0$) along the (111) direction (top panel) and along the (1-10) direction (bottom panel). The classical case with no averaging over zero-point vibration is shown by the dotted line. The SCH approach with quantum averaging is shown for both H$_2$ (dashed) and D$_2$ (solid). Note that the isotope effect is significantly renormalized from the expected value of $\sqrt{2}$.

which the rotational levels, phonon states, etc. are calculated by averaging over the zero-point motion of the ground-state phonon wave function. Figure 11 shows the potential energy for a H$_2$ molecule translating along the [111] and [1-10] direction.[19] At the same time it is necessary to consider the orientation of the H$_2$ molecule. The particular curves shown are calculated for the case in which the molecule is in the $J=0$ rotational state (spherically symmetric). First we consider a classical harmonic model (dotted line) in which zero-point motion is neglected. The curvature of the potential function yields frequencies $\omega_A \approx 9.64$ meV (top panel) and $\omega_E \approx 10.95$ meV (bottom panel), respectively. These values are much smaller than those of the experimental peaks, shown in Fig. 8, which are on the order of 14 meV. In addition, the calculated frequencies predict a very large mean-square amplitude for the zero-point motion

$$\langle u^2 \rangle \approx \frac{3\hbar}{2m\omega} \approx 0.2 \ \text{Å}^2 \qquad (6)$$

and hence, the classical harmonic approximation is shown to be seriously inadequate and we must use a full quantum-mechanical approach.

The first approximation is to average the anisotropic interaction $V(\mathbf{R},\mathbf{\Omega})$ over the range of the zero-point motion of a H$_2$ molecule while keeping the orientation, $\mathbf{\Omega}$, fixed. We denote the resulting potential by $\bar{V}(\mathbf{r},\mathbf{\Omega})$ which represents the static renormalization of $V(\mathbf{r},\mathbf{\Omega})$ as a result of the zero-point motion, where ''static'' refers to the averaging being performed for constant $\mathbf{\Omega}$;

$$\bar{V}(\mathbf{r},\mathbf{\Omega}) = \langle 0|V(\mathbf{R},\mathbf{\Omega})|0\rangle, \qquad (7)$$

where $\mathbf{r}$ now represents the center of the *zero-point motion distribution* of the H$_2$ molecule and can be used as an appropriate expansion parameter. In order to perform the required averaging, we introduce a simple model for the zero-point motion. We assume that it can be described by a Gaussian distribution corresponding to the ground state of a simple harmonic oscillator:

$$|0\rangle = Ne^{-(1/2)\sum_{\alpha,\beta} u_\alpha G_{\alpha,\beta} u_\beta}, \qquad (8)$$

where N is the normalization constant and the matrix G contains the anisotropic parameters, which define the spatial distribution of the zero-point vibrations. The square root of G is related to the dynamical matrix of the system from which the normal modes are calculated and in turn the new ground-state wave function. As described in Appendix B (the SCH approach) these calculations are repeated iteratively until we obtain self-consistent values for G.

By modeling the zero-point motion with a Gaussian distribution we are able to perform the averaging procedure analytically. The obtained values are accurate to the desired order of $\langle u^2 \rangle / d^2$ where $\langle u^2 \rangle$ is the mean-square value for the zero-point motion and d is the average distance between the center of the H$_2$ molecule and the carbon atoms of the C$_{60}$ molecules. For our particular system, this ratio is about 0.02, and we perform the expansion to second order. The analytical expression for the renormalized potential, $\bar{V}(\mathbf{r},\mathbf{\Omega})$, to second order is derived in Appendix B and given by

$$\bar{V}(\mathbf{r},\mathbf{\Omega}) = \sum_{i \in H_2} \sum_{j \in C_{60}} \{B(r_{ij})e^{-Cr_{ij}} - A(r_{ij})/r_{ij}^6\}, \qquad (9)$$

where $B(r_{ij})$ and $A(r_{ij})$ are the renormalized parameters given as

$$B(r) = B \times \left(1 + \frac{1}{2} \sum_{\alpha,\beta} \langle 0|u_\alpha u_\beta|0\rangle \right.$$
$$\left. \times \left\{ \left[\frac{1}{r}+C\right]\frac{Cr_\alpha r_\beta}{r^2} - \frac{\delta_{\alpha,\beta}C}{r} \right\} \right),$$

$$A(r) = A \times \left(1 + \sum_{\alpha,\beta} \langle 0|u_\alpha u_\beta|0\rangle \left\{ \frac{24 r_\alpha r_\beta}{r^4} - \frac{3\delta_{\alpha,\beta}}{r^2} \right\} \right). \qquad (10)$$

The net result of this zero-point averaging is to modify the C-H interactions by up to 30% from that of the classical model. The solid (dashed) line in Fig. 11 shows the radial part of the renormalized potential along [111] (top panel) and [1-10] (bottom panel) directions for the case of H$_2$ (D$_2$) in the $J=0$ rotational state. Comparing the classical and quantum case, we see that the renormalized potentials are much stiffer for both H$_2$ and D$_2$. The renormalized phonon frequencies are now around 14.9 and 10.0 meV for H$_2$ and D$_2$, respectively. The self-consistent values of the $\langle u_\alpha u_\beta \rangle$, the phonon frequencies and the zero-point energies (ZPE's) for $|JM\rangle$ states are are listed in Table II. These values are now in good

TABLE II. Self-consistent values of the $\langle u_\alpha u_\beta \rangle$ and the corresponding local phonon modes (in meV) of H$_2$ (left) and D$_2$ (right) molecules trapped in the octahedral site of solid C$_{60}$ with $Pa\bar{3}$ ordering. ω_A and ω_E represent the single and double degenerate phonons, respectively. The last columns of the left (H$_2$) and right (D$_2$) panels of the table give the zero-point energy (ZPE$=\frac{1}{2}\Sigma_i\omega_i$) from which the additional splitting and downward shift of the center of gravity (CG) of the $|JM\rangle$ levels are apparent.

		H$_2$					D$_2$			
$|JM\rangle$	$\langle u_\alpha^2 \rangle$	$\langle u_\alpha u_\beta \rangle$	ω_A	ω_E	$\frac{1}{2}\Sigma_i\omega_i$	$\langle u_\alpha^2 \rangle$	$\langle u_\alpha u_\beta \rangle$	ω_A	ω_E	$\frac{1}{2}\Sigma_i\omega_i$
00	0.0664	0.0020	13.62	14.92	21.72	0.0499	0.0016	9.02	9.93	14.44
10	0.0668	0.0023	13.43	14.60	21.31	0.0503	0.0019	8.89	9.67	14.11
1±1	0.0662	0.0019	13.51	14.73	21.48	0.0498	0.0015	9.08	9.88	14.43

agreement with the experimental data presented in the previous section. The isotope effect from our calculations is now

$$\left(\frac{\omega_{H_2}}{\omega_{D_2}}\right)^2 \approx 2.3, \tag{11}$$

which is significantly larger than the classical value of 2.0 and in good agreement with the observed value of 2.2. This large isotope effect occurs because the lighter mass of H$_2$ leads to a large zero-point motion and therefore a significantly larger renormalization of the parameters in the interaction potential while for D$_2$, the renormalization effect is reduced and for much larger molecules, such as CH$_4$, the effect of the zero-point motion is negligible and hence the SCH approach is reduced to the classical case.

C. Rotational levels

Next we study the splitting of the rotational J levels due to interaction potential $\bar{V}(\mathbf{r},\mathbf{\Omega})$ where we again have to consider the effect of the zero-point motion. Figure 12 shows the projection of the five-dimensional potential, $V(\mathbf{R},\mathbf{\Omega})$, in $\theta - \phi$ plane. This projection describes the potential felt by the H$_2$ molecule in terms of its orientation. In the left panel we show the potential contour plot for the high-temperature phase in which the C$_{60}$ molecules are orientationally disordered and, therefore, the potential has O$_h$ symmetry. The analytical form of the potential assuming spherically disordered C$_{60}$ molecules is given in Appendix A. Consistent with O$_h$ symmetry, there are eight minima along [111] axes. The [100] orientations for H$_2$ correspond to the maxima in the potential. We note that the barrier between these minimum and maximum orientations is on the order of 1 meV, which is much smaller than the energy difference between the rotational J levels, and therefore the orientational dependence of the potential is a small perturbation to free rotor behavior.

The right panel in Fig. 12 shows the potential in the low-temperature phase when the C$_{60}$ molecules are ordered as in $Pa\bar{3}$ with a setting angle of 24°.[11,12] The potential symmetry is now reduced to that of S$_6$ and only two (the threefold axis of the S$_6$ symmetry) of the eight [111] orientations are still
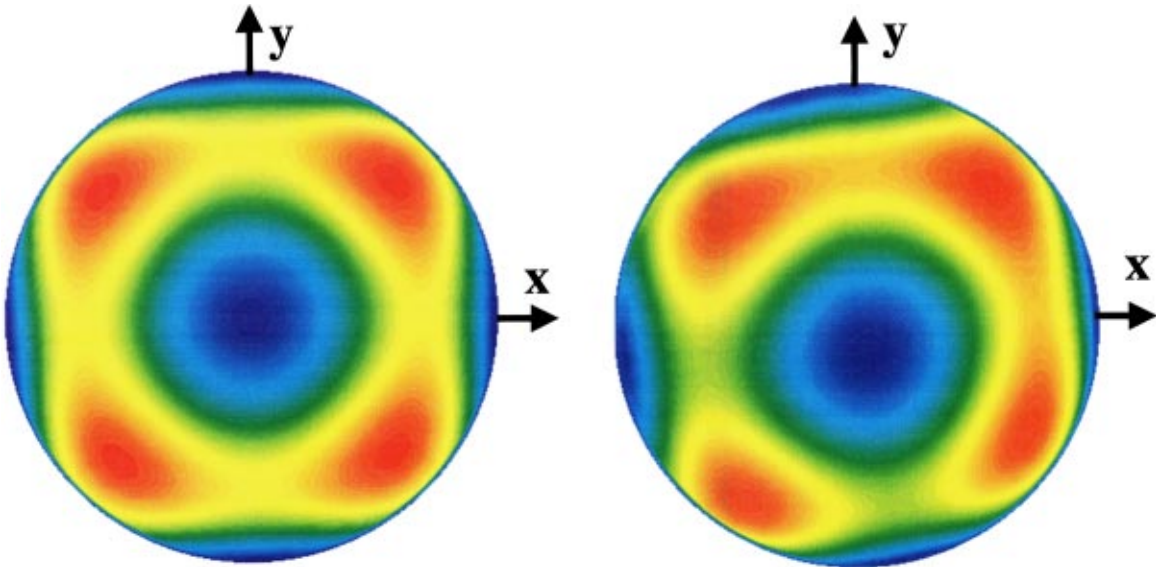

FIG. 12. (Color) Contour plot of the orientational potential energy surface of H$_2$ molecule (as viewed along the z axis) when the surrounding C$_{60}$ molecules are spherically disordered (left panel, local symmetry is O$_6$) and orientationally ordered as in $Pa\bar{3}$ (right panel, site symmetry is S_6). Colors from red to blue show the variation of the potential energy surface from -109 to -111 meV. When the C$_{60}$ molecules are disordered (left) we have eight minima along the (111) directions and six maxima at the (100) directions, which are separated by a potential barrier of about 1 meV. When C$_{60}$ molecules are ordered (right), the threefold axis of the S$_6$ symmetry becomes the global minimum while the others become local minima.

TABLE III. The values of the expansion parameters V_{lm} of the potential $\bar{V}(r,\Omega)$ given in Eq. (16) when C$_{60}$ molecules are orientationally ordered ($Pa\bar{3}$) and disordered ($Fm\bar{3}m$). The z axis is taken to be along the threefold axis for both cases. $\Delta_{CF}=\sqrt{9/20\pi}V_{20}$ is the splitting of the $|00\rangle$ and $|1\pm1\rangle$ levels due to the crystal field. Δ_T is the total splitting due to both crystal field and ZPE which is obtained from Table II.

$\bar{V}(r,\Omega)$	$Pa\bar{3}$			$Fm\bar{3}m$		
	SCH (H$_2$)	SCH (D$_2$)	Clas. (H$_2$,D$_2$)	SCH (H$_2$)	SCH (D$_2$)	Clas. (H$_2$,D$_2$)
V_{00} (meV)	-109.3	-110.6	-114.6	-102.4	-105.3	-114.4
V_{20} (meV)	-1.20	-1.10	-0.82	0	0	0
V_{40} (meV)	-0.40	-0.37	-0.28	-0.59	-0.54	-0.38
α_c	0.845	0.843	0.835	1	1	1
α_s	1.941	1.944	1.956	1	1	1
Δ_{CF} (meV)	0.45	0.42	0.31			
Δ_T (meV)	0.62	0.74	0.31			

minima. As shown below the effect of $Pa\bar{3}$ ordering can be well described by adding the spherical harmonic term $Y_2^m(\theta,\phi)$ to the total potential. The variation with H$_2$ orientation however, is still perturbatively small and the H$_2$ rotations are so little hindered that the single molecular rotational properties can still be described in terms of the molecular rotational quantum numbers $|JM\rangle$.

To calculate the actual energy of the levels we start by expanding the intermolecular potential in terms of spherical harmonics

$$\bar{V}(\mathbf{r},\Omega)=\sum_l \sum_{m=-l}^{l} V_{lm}Y_l^m(\Omega),\qquad(12)$$

where V_{lm} is radial value for each angular component l and m at the equilibrium position of the CM of H$_2$. The rotational levels of the H$_2$ molecules can then be obtained by diagonalizing the Hamiltonian

$$\langle JM|H|J'M'\rangle=BJ(J+1)\delta_{J,J'}\delta_{M,M'}+\sum_l \sum_{m=-l}^{l} V_{lm}$$

$$\times\sqrt{\frac{(2J+1)(2J'+1)(2l+1)}{4\pi}}$$

$$\times(-1)^M\begin{pmatrix} J & l & J' \\ -M & m & M' \end{pmatrix}\begin{pmatrix} J & l & J' \\ 0 & 0 & 0 \end{pmatrix},$$

$$(13)$$

where the last two factors are the Wigner $3j$ symbols.[20]

Most of the terms in the above expansion vanish due to the high symmetry of the potential. For spherically disordered C$_{60}$, the local symmetry is O$_h$ and, therefore, the leading terms in a reference frame where the z axis is the threefold axis (which is more convenient than fourfold axis to make the comparison with the $Pa\bar{3}$ case) are

$$\bar{V}(\mathbf{r},\Omega)=V_{00}+V_{40}\left[Y_4^0(\Omega)+\sqrt{\frac{10}{7}}[Y_4^{3,c}(\Omega)+Y_4^{3,s}(\Omega)]\right],$$

$$(14)$$

where the values of V_{00} (binding energy of H$_2$ to the octahedral site) and V_{40} are listed in Table III with and without

zero-point averaging for both H$_2$ and D$_2$. Here $Y_4^{3,c}(\Omega)$ and $Y_4^{3,s}(\Omega)$ are defined as

$$Y_l^{m,c}=\frac{1}{\sqrt{2}}[Y_l^m+Y_l^{m*}],\quad Y_l^{m,s}=\frac{-i}{\sqrt{2}}[Y_l^m-Y_l^{m*}],\quad(15)$$

where $Y_l^{m*}=(-1)^m Y_l^{-m}$.

In the left panel of Fig. 13 we show the splitting of the J levels as a function of V_{40} where the vertical solid and dotted lines indicate the calculated values of V_{40} with and without zero-point averaging. Due to the triangular closure relation of the final term in Eq. (13) the lowest J value that is split by
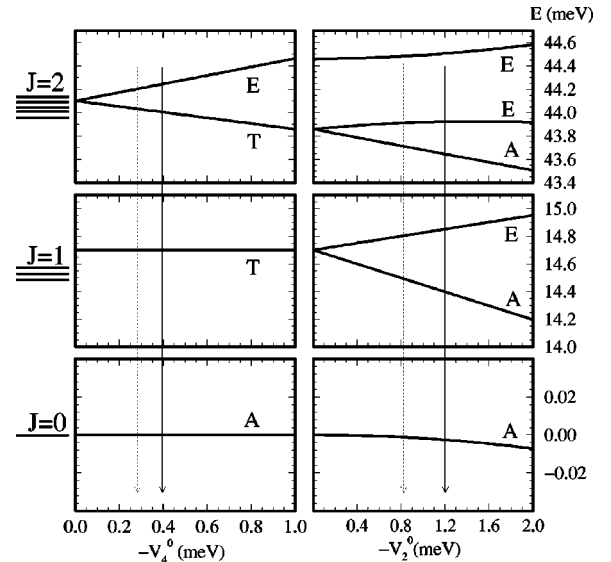

FIG. 13. A schematic representation of the splitting of the J levels due to the crystal-field effect. The left panel applies to the high-temperature phase with orientationally disordered C$_{60}$ molecules in which the potential has O$_h$ symmetry and does not split the $J=1$ levels. The right panel shows the additional splitting that occurs in the low-temperature phase as a result of the orientational ordering of the C$_{60}$ molecules. The vertical solid and dotted lines represent the calculated values of the parameters V_{20} and V_{40} with and without zero-point-averaging, respectively. Here A, E, and T indicate that the states are singly, doubly, and triply, degenerate respectively.

an octahedral potential is $J=2$. Thus, in the high-temperature phase the $J=1$ levels maintain their degeneracy. However, they are subject to splitting when we impose the low-temperature orientational ordering of the C_{60} molecules. For a perfect $Pa\bar{3}$ ordering, the local symmetry is reduced to S_6 and the leading terms in the expansion of the potential are now

$$\bar{V}(\mathbf{r},\mathbf{\Omega}) = V_{00} + V_{20}Y_2^0(\mathbf{\Omega})$$
$$+ V_{40}\left[Y_4^0(\mathbf{\Omega}) + \sqrt{\frac{10}{7}}(\alpha_c Y_4^{3,c}(\mathbf{\Omega}) + \alpha_s Y_4^{3,s}(\mathbf{\Omega}))\right]$$
$$(16)$$

where the z axis is the threefold axis of the S_6. Numerical values of the V_{00}, V_{20}, V_{40}, α_c, and α_s for our particular potential are listed in Table III. The second term in the above expansion of the crystal-field (CF) potential is responsible for the splitting of the $J=1$ levels;

$$\Delta_{CF} = E_{|1\pm1\rangle} - E_{|10\rangle} = -\sqrt{\frac{9}{20\pi}}V_{20}. \quad (17)$$

From Table III we note that the SCH approach is essential to get the required splitting. CF splits the levels by roughly 0.45 meV for H_2 and 0.42 meV for D_2. The zero-point energy ($\frac{1}{2}\Sigma_i\omega_i$ shown in Table II) shows that the levels are further split due to dependence of the ZPE on the $|JM\rangle$ states. When Δ_{CF} is combined with this we obtain a splitting on the order of 0.7 meV for both H_2 and D_2, in excellent agreement with the experimental results.

In the right panel of Fig. 13 we show how the splitting of the J levels develop as V_{20} is tuned (while keeping $V_{40} = 1$ meV and $\alpha_c = \alpha_s = 1$.) Again the solid and dotted lines indicate the calculated values with and without zero-point renormalization. Once renormalization is included, the calculated splitting of the $J=1$ levels agree quite well with the experimental observation. However, despite this good agreement, the calculations show the center of the gravity (CG) of the J levels as unchanged which is in marked contrast to the experimental observations which show a 0.35 and 0.15 meV downward shift in the CG of the $J=1$ levels, for H_2 and D_2, respectively.

The reason for this downward shift is not immediately obvious. Since the potential contains inversion symmetry, there are no terms in the expansion with odd l. Thus the matrix element $\langle JM|H|J'M'\rangle$ is zero unless both J and J' are odd or even. In addition, coupling within a single J manifold can never lead to a shift in the CG. Therefore, the highest term that could lead to a shift is the matrix elements linking the $J=0$ and $J=2$ states. However, in this case these levels are widely separated resulting in extremely weak coupling and therefore any shift in the CG should be very small. In fact, the bottom panel of Fig. 13 indicates that due to this tiny coupling between $J=0$ and $J=2$ states, the $J=0$ level is shifted downward by less than 0.01 meV. To explain the observed shift we once more have to consider the effects of the zero-point motion of the H_2 molecules. The ground state and thus the phonon frequencies of the H_2 molecule are different for the different $|JM\rangle$ states. Hence, they have different zero-point energy (ZPE$=\frac{1}{2}\Sigma_i\omega_i$). When a transition is

made from a $J=0$ to a $J=1$ state these differences in the ZPE have to be included. In Table II we show the normal modes of the H_2 molecule and the corresponding ZPE for different $|JM\rangle$ states. From this table one sees that the CG of the $J=1$ levels are shifted downward by about 0.3 meV for H_2 and 0.12 meV for D_2, in good agreement with our experimental values of 0.45 and 0.15 meV, respectively.

Finally, we note that normal modes of the H_2 molecule depend upon its angular state. Hence the phonon density of states observed by neutron scattering should contain peaks, at the various energies listed in Table II. Our calculations predict phonon modes at energies from 14.4 to 15 meV, which is in good agreement with the QENS data shown in Fig. 8. The relative intensities of these modes are determined by the appropriate ortho and para concentrations. Although our calculations predict a set of phonons in roughly the correct energy range, complete assignment of the QENS features shown in Fig. 8 was not possible. However, comparing phonon energies listed in Table II and Fig. 8, it is tempting to conclude that the features observed at energies of 13.5 and 15 meV are the phonons corresponding to vibrations of H_2 parallel and perpendicular to the $\langle 111\rangle$ axis, respectively. The feature observed around 14.0 meV would be then a superposition of the rotational and remaining phonon excitations. Perhaps one of the reasons for the failure of our calculations to assign the features unambiguously is that we have neglected the fact that some of the C_{60} molecules are not in their equilibrium $Pa\bar{3}$ orientations. In fact, it is known that 1/6 are in a defect orientation,[11] which lowers the local symmetry. Currently, we are trying to incorporate the effect of these defect orientations into a more complete model in which we solve the five-dimensional Schrodinger equation for the bound states of the H_2 molecule rather that using the SCH approach outlined above. It is hoped that by doing this we will be able to fully explain the various features present in the spectrum shown in Fig. 8.

V. SUMMARY

We have presented a detailed experimental and theoretical study of the quantum dynamics of H_2 and D_2 trapped at the interstitial sites of solid C_{60} with emphasis on the transitions between the rotational levels and the density of phonon states. Our conclusions can be summarized as follows:

The sorption of hydrogen into solid C_{60} forms a system in which one can study a simple quantum object trapped in a classical matrix. Measuring H_2 uptake as a function of pressure yielded a loading isotherm which is shown to deviate significantly from a standard Langmuir response and follows instead an exponential form, increasing from 40% filling at 130 atm to 90% at 700 atm.

The elastic neutron-scattering results expressed as a difference Fourier transform analysis of the $C_{60}(D_2)_x$ diffraction data clearly show the D_2 molecules situated randomly at the O sites without any long-range order. Inelastic neutron-scattering results indicate that the interstitial molecules form a system in which the potential is quite rigid for center-of-mass translation while at the same time being very soft for rotational motion.

We clearly observed the ortho to para conversion of the interstitial hydrogen, which occurs via a transition from the
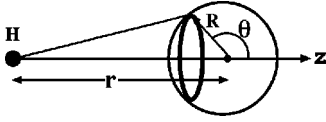
FIG. 14. A schematic representation of the local reference frame in which the interaction between a hydrogen atom and a C_{60} molecule is integrated over the C_{60} orientation. After integration, the final interaction is solely a function of the distance between the H atom and the center of the C_{60} molecule.

$J=1$ to $J=0$ rotational levels. The excited level is shown to be both split, 0.7 meV and shifted in energy, by 2%, from that of free H_2. We also identify the translational modes of the trapped H_2 which are remarkably high in energy and have an isotopic shift on the order of $\sqrt{2.2}$.

This behavior is shown to be due to large zero-point motions of the H_2 molecules in the O sites, leading to a significant departure from classical predictions. The coupling between the rotational and the vibrational motion of the molecule (zero-point motion), arising from the dependence of the anisotropic intermolecular forces on the H-C distance, gives rise to a downward shift and additional splittings of the rotational levels as observed in the INS data.

The neutron energy-loss data (see Fig. 8) indicates a range of features whose identification requires further study. Similar experiments for D_2 would be very useful in identifying these detailed features and would also provide precise information about the local potential felt by the H_2 molecule. This in turn would provide information about the defect orientation of the C_{60} molecules in the ordered phase.

Other techniques such as proton NMR and specific heat should prove very interesting in studying this system. Due to the splitting of the $J=1$ levels there should be a Shottky anomaly around $T \approx \Delta/k$, where Δ is the splitting of the $J=1$ levels. It would be interesting to study the effects of pressure on the system and in particular to determine whether the influence of an external pressure on the C_{60} lattice can cause the H_2 motion to change from that of a weakly hindered rotation to that of a confined librational oscillator in a well-defined potential well.

APPENDIX A: INTERMOLECULAR POTENTIAL DUE TO ORIENTATIONALLY DISORDERED C₆₀

In this appendix we perform an averaging over the C_{60} orientation for the pair-wise potential listed in Eq. (5). For this purpose, it is sufficient to consider interaction between a hydrogen atom and a spherically disordered C_{60} molecule as shown in Fig. 14. The total interaction is the summation of this interaction over two hydrogen atoms and the nearest-neighbor C_{60} molecules. As shown in Fig. 14, we chose the reference frame such that the z axis is the line connecting the hydrogen atom to the center of the C_{60} molecule. Then, the interaction between the hydrogen atom and a spherically disordered C_{60} can be written in integral form as

$$V(r) = \frac{60}{4\pi R^2} \int_0^\pi d\theta \sin(\theta) f(\sqrt{r^2 + R^2 + 2rR \cos(\theta)}),$$
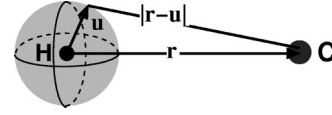
(A1)

FIG. 15. A schematic representation of the interaction between a carbon atom and a hydrogen atom which due to zero-point vibrations can be anywhere within the large grey sphere. The instantaneous interaction is a function of $|\mathbf{r}-\mathbf{u}|$. However, after averaging over the zero-point motion $\mathbf{u}$, the final renormalized interaction depends solely upon $\mathbf{r}$, the vector joining the center of zero-point motion distribution to the carbon atom. As discussed in the text, this renormalization modifies interaction parameters significantly.

where R and r are the radius of the C_{60} and the radial distance between the hydrogen atom and the C_{60} center, respectively. Here $f(r)$ is the two-body pairwise potential, which contains the two terms $1/r^6$ and e^{-Cr}.

For $f(r) = 1/r^{2n}$ (where n can be three, six, etc.), one obtains the result

$$V_{2n}(r) = \frac{15}{rR(n-1)} \left(\frac{1}{(r-R)^{2(n-1)}} - \frac{1}{(r+R)^{2(n-1)}} \right).$$

(A2)

Similarly, for $f(r) = Be^{-Cr}$, one gets

$$V_{\exp}(r) = \frac{30Be^{-Cr}}{rRC} \left[\left(\frac{1}{C} + r - R \right) e^{CR} - \left(\frac{1}{C} + r + R \right) e^{-CR} \right].$$

(A3)

Using these expressions, one can easily calculate the potential felt by the H_2 molecule in the octahedral field of the surrounding spherically disordered C_{60} molecules.

APPENDIX B: RENORMALIZATION OF THE INTERMOLECULAR POTENTIAL DUE TO ZERO-POINT VIBRATION OF H₂ AND SELF-CONSISTENT HARMONIC APPROACH

In this appendix, we first calculate the renormalization of the potential due to the zero-point vibration of the H_2 molecule and then we present the phonon calculations within the self-consistent harmonic approach. We assume a rigid H_2 molecule whose center of mass performs a zero-point vibration described by a Gaussian distribution as stated in Eq. (8). Since the molecule is rigid, it is only necessary to obtain the expression for the renormalization due to the effect of the zero-point motion on the interaction between a single hydrogen atom and a carbon site on the C_{60} molecule. The total interaction is then given simply by the sum of the interactions between the two hydrogen atoms and all the carbon atoms of the six neighboring C_{60} molecules. We assume that the instantaneous interaction between H and C sites is given by

$$V_{\text{CH}}^{\text{ins}}(R) = f(|\mathbf{r}-\mathbf{u}|),$$

(B1)

where $f(r)$ is the potential function, $\mathbf{u}$ is the displacement vector of the hydrogen atom due to zero-point vibration, and r is the distance between the center of zero-point motion and the carbon atom. The situation is schematically shown in Fig. 15. For our particular system of H_2 trapped in the octahedral

site, the ratio of $(u/r)^2$, given by $(u/r)^2 = (0.24/3.5^2) = 0.02$, is small enough that it can be used as an expansion parameter.

The normalized interaction is the average of the instantaneous interactions, given in Eq. (B1), over the zero-point motions of the H atoms. Hence, the normalized potential is given as

$$\bar{V}_{\text{CH}}(r) = \int d^3 u |\Psi(u)|^2 V_{\text{CH}}^{\text{ins}}(R) = \langle 0|f(|\mathbf{r} - \mathbf{u}|)|0\rangle, \tag{B2}$$

where Ψ is the Gaussian function describing the zero-point vibration listed in Eq. (8), which is determined self-consistently within SCH approach as described below.

Using Taylor expansion, we can write

$$f(|\mathbf{r} - \mathbf{u}|) = f(r) - \sum_\alpha \frac{r_\alpha}{r} f'(r) u_\alpha + \frac{1}{2} \sum_{\alpha,\beta} \left[\frac{r_\alpha r_\beta f''(r)}{r^2} \right.$$
$$\left. + \left(\delta_{\alpha,\beta} - \frac{r_\alpha r_\beta}{r^2} \right) \frac{f'(r)}{r} \right] u_\alpha u_\beta + O((u/r)^3), \tag{B3}$$

where α, β are the Cartesian components, $f'(r)$ and $f''(r)$ are the first and second derivative of $f(r)$, respectively, and r_α is the αth component of $\mathbf{r}$. Averaging this expansion over the zero-point vibration of the H atom yields

$$\bar{V}_{\text{CH}}(r) = f(r) + \frac{1}{2} \sum_{\alpha,\beta} \left[\frac{r_\alpha r_\beta f''(r)}{r^2} + \left(\delta_{\alpha,\beta} - \frac{r_\alpha r_\beta}{r^2} \right) \frac{f'(r)}{r} \right]$$
$$\times \langle 0|u_\alpha u_\beta|0\rangle. \tag{B4}$$

Here the linear term in u vanishes due to the inversion symmetry of the Gaussian distribution assumed for the zero-point motion.

Now, for the first term of $f(r), A_{2n}/r^{2n}$, we have

$$\langle 0|A_{2n}/r^{2n}|0\rangle = A_{2n}(r)/r^{2n}, \tag{B5}$$

where

$$A_{2n}(r) = A_{2n} \left(1 + \sum_{\alpha,\beta} \left[\frac{2n(n+1)}{r^4} r_\alpha r_\beta - \frac{n}{r^2} \delta_{\alpha,\beta} \right] \right.$$
$$\times \langle 0|u_\alpha u_\beta|0\rangle \right). \tag{B6}$$

For the second term, Be^{-Cr}, we have

$$\langle 0|Be^{-Cr}|0\rangle = B(r)e^{-Cr}, \tag{B7}$$

where the renormalized potential parameter $B(r)$ is

$$B(r) = B \left(1 + \frac{1}{2} \sum_{\alpha,\beta} \left[\frac{r_\alpha r_\beta C}{r^2} \left[\frac{1}{r} + C \right] - \frac{C}{r} \delta_{\alpha,\beta} \right] \right.$$
$$\times \langle 0|u_\alpha u_\beta|0\rangle \right). \tag{B8}$$

The last term $\langle 0|u_\alpha u_\beta|0\rangle$ in the equations above is related to the matrix $G = (G_{\alpha,\beta})$ given in Eq. (8) in terms of the eigenvalues (ω_α) and the vectors (U) of the local vibrational modes of the H_2 molecule. Renormalization of the potential proceeds via an initial guess for $\langle 0|u_\alpha u_\beta|0\rangle$ which is used to calculate the potential given above. Then the renormalized dynamical matrix is calculated numerically using finite displacement technique:

$$\bar{D}_{\alpha,\beta} = (\delta^2 \bar{V}(r)/\delta r_\alpha \delta r_\beta), \tag{B9}$$

and the corresponding eigenvectors and values are calculated from the resulting dynamical matrix $\bar{D}$;

$$\bar{D} U = \omega U. \tag{B10}$$

The above eigenvalues and eigenvectors are then used iteratively to update the expectation values of the displacements,

$$\langle 0|u_\alpha u_\beta|0\rangle = \frac{\hbar}{2m} \sum_\gamma U_{\alpha,\gamma} U_{\beta,\gamma}/\omega_\gamma. \tag{B11}$$

This procedure is repeated with a new input of $\langle 0|u_\alpha u_\beta|0\rangle$ which is obtained by mixing the previous and current values (to accelerate the convergence). The self-consistency is assumed to be obtained when the current values of the $\langle 0|u_\alpha u_\beta|0\rangle$ do not change significantly from the previous values. The details of this *self-consistent harmonic* approach are given in Refs. 21–23.

A final remark is that for isotropic zero-point vibration (such as one in the octahedral crystal field of orientationally disordered C_{60} molecules), the average $\langle 0|u_\alpha u_\beta|0\rangle$ is simply given as

$$\langle 0|u_\alpha u_\beta|0\rangle = \frac{1}{3} \langle u^2\rangle \delta_{\alpha,\beta}, \tag{B12}$$

which simplifies the above renormalization equations considerably. However, for our purpose where C_{60} molecules are orientationally ordered with local S_6 symmetry, we cannot use this simplification and we have to consider the full anisotropic Gaussian function.

[1] R.A. Assink, J.E. Schirber, D.A. Loy, B. Morosin, and G.A. Carlson, J. Mater. Res. **7**, 2136 (1992).

[2] S.A. FitzGerald and A.J. Sievers, J. Chem. Phys. **101**, 7283 (1994).

[3] J.E. Schirber, G.H. Kwei, J.D. Jorgensen, R.L. Hitterman, and B. Morosin, Phys. Rev. B **51**, 12 014 (1995).

[4] B. Morosin, J.D. Jorgensen, S. Short S, G.H. Kwei, and J.E. Schirber, Phys. Rev. B **53**, 1675 (1996).

[5] I. Holleman, G. von Helden, E.H.T. Olthof, P.J.M. van Bentum, R. Engeln, G.H. Nachtegaal, A.P.M. Kentgens, B.H. Meier, A. van der Avoird, and G. Meijer, Phys. Rev. Lett. **79**, 1138 (1997).

[6] I. Holleman, G. von Helden, A. van der Avoird, and G. Meijer,

Phys. Rev. Lett. **80**, 4899 (1998).

[7] I.F. Silvera, in *Proceedings of the 14th International Conference on Low Temperature Physics*, Otaniemi, Finland, 1975, edited by M. Krusius and M. Vuorio (North-Holland, Amsterdam, 1975), Vol. 5, p. 123.

[8] J.K. Stalick *et al.* in *Neutron Scattering in Materials Science II*, edited by D. A. Newmann *et al.*, MRS Symposia Proceedings No. 376 (Materials Research Society, Pittsburgh, 1994), p. 101.

[9] J.R.D. Copley and T.J. Udovic, J. Res. Natl. Inst. Stand. Technol. **98**, 71 (1993).

[10] A. Bondi, J. Phys. Chem. **68**, 441 (1964).

[11] W.I.F. David, R.M. Ibberson, J.C. Matthewman, K. Prassides, T.J.S. Dennis, J.P. Hare, H.W. Kroto, R. Taylor, and D.R.M. Walton, Nature (London) **353**, 147 (1991).

[12] R. Sachidanandam and A.B. Harris, Phys. Rev. Lett. **67**, 1467 (1991); P.A. Heiney *et al.*, *ibid.* **67**, 1468 (1991).

[13] General Structure Analysis System (GSAS), A. C. Larson and R. B. Von Dreele, Los Alamos National Laboratory Report No. LAUR 86-748.

[14] Since the scattering is dominated by carbon atoms, we could not distinguish between models in which D_2 is treated as point object versus those in which it is treated as a hollow sphere. Thus we choose to model D_2 as a point object in which the refined temperature factors are used to estimate the rms displacement of this point object.

[15] B.P. Stoicheff, Can. J. Phys. **35**, 730 (1957).

[16] I.F. Silvera, Rev. Mod. Phys. **52**, 393 (1980).

[17] J.A. Young and J.U. Koppel, Phys. Rev. **135**, A603 (1964).

[18] *The Atom-Atom Potential Method*, edited by A. J. Pertsin and A. I. Kitaigorodsky (Springer-Verlag, Berlin, 1986).

[19] In the classical case, some of the potentials are minimized when the center of the H_2 molecule in the octahedral site is located off center. However, the phonons of the H_2 molecule at this off-center position are still found to be very small compared to experimental data. In contrast, after zero-point averaging all the potentials that we tested are optimized when H_2 is centered at the octahedral site with phonon energies which are much closer to experimental values.

[20] M. Rotenberg, R. Bivins, N. Metropolis, and J. K. Wooten, Jr., *The 3j- and 6j- symbols* (Technology Press, MIT, Cambridge, MA, 1959); B. R. Judd, *Angular Momentum Theory for Diatomic Molecules* (Academic, New York, 1975).

[21] T.R. Koehler, Phys. Rev. Lett. **17**, 89 (1966).

[22] *Dynamical Properties of Solids*, edited by G. H. Horton and A. A. Maradudin (American Elsevier, New York, 1975); *Rare Gas Solids*, edited by M. L. Klein and J. A. Venables (Academic, London, 1976).

[23] J. Van Kranendonk, *Solid Hydrogen* (Plenum, New York, 1983).